

1           **Molecular emission in laser-induced breakdown spectroscopy: an**  
2           **investigation of its suitability for chlorine quantification on Mars**

3  
4 D. S. Vogt<sup>1</sup>, K. Rammelkamp<sup>1</sup>, S. Schröder<sup>1</sup>, H.-W. Hübers<sup>1,2</sup>

5 <sup>1</sup>Deutsches Zentrum für Luft- und Raumfahrt (DLR), Institute of Optical Sensor Systems, Berlin,  
6 Germany.

7 <sup>2</sup>Humboldt-Universität zu Berlin, Department of Physics, Berlin, Germany.  
8

9 Corresponding author:

10 David S. Vogt

11 Rutherfordstraße 2

12 12489 Berlin, Germany

13 +49 30 67055-427

14 david.vogt@dlr.de  
15

16 **Keywords:** Spectroscopy, Mars, Experimental techniques

17 **Abstract**

18       The intensity of the molecular CaCl emission in LIBS spectra is examined in order to evaluate  
19 its suitability for the detection of chlorine in a Martian environment. Various mixtures  
20 resembling Martian targets with varying Cl content are investigated under simulated Martian  
21 conditions. The reactions leading to the formation of CaCl are modeled based on reaction  
22 kinetics and are used to fit the measured CaCl band intensities. MgCl bands are also investigated  
23 as potential alternatives to CaCl, but no MgCl bands can be identified in samples containing both  
24 Mg and Cl. The study confirms that CaCl is well suited for the indirect detection of chlorine, but  
25 finds a strong dependence on the concentrations of Ca and Cl in the sample. Spectra from  
26 samples with a high chlorine concentration can have low-intensity CaCl emission due to a  
27 deficiency of Ca. A qualitative estimate of the sample composition is possible based on the ratio  
28 of the band intensity of CaCl to the intensity of Ca emission lines. Time-resolved measurements  
29 show that the CaCl concentration in the plasma is highest after about 1  $\mu$ s.

## 30 **1. Introduction**

31 Chlorine plays an important role in the research of Martian geology. Studies of Martian  
32 meteorites (Dreibus and Wänke, 1985) and remote sensing measurements of the Martian surface  
33 (Keller et al., 2006; Taylor et al., 2010) have shown significant enrichments in chlorine, leading  
34 Dreibus and Wänke to suggest that the chlorine concentration of Mars is about three times higher  
35 than that of Earth (Dreibus and Wänke, 1987). The heterogeneous distribution of chlorine at the  
36 Martian surface has been linked to geological processes such as hydrothermal and volcanic  
37 activity (Keller et al., 2006). It has also been suggested that, instead of water, chlorine was the  
38 dominant volatile species in Martian magmas (Filiberto and Treiman, 2009). Additionally,  
39 chlorides and perchlorates are important salts in the search for liquid water on Mars. Aqueous  
40 solutions with salts have a lower freezing point and reduced equilibrium vapor pressure, which  
41 leads to an increased stability of the solution (Haberle et al., 2001; Rennó et al., 2009; Smith et  
42 al., 2009). Therefore, precipitates of salts are expected in areas where water has evaporated in the  
43 past. Both chlorides and perchlorates are among the salts that have been detected remotely and  
44 in-situ on the surface of Mars (Ehlmann and Edwards, 2014; Hecht et al., 2009; Massé et al.,  
45 2010; Osterloo et al., 2008). The detection of chlorine is important for a more complete  
46 understanding of early Mars, present Martian environments, and the history of water on Mars.  
47 This remains a major goal for current and future Mars missions.

48 The NASA Mars Science Laboratory (MSL) Curiosity rover has been successfully operating  
49 at Gale crater since August 2012, with the goal of searching for habitable environments  
50 (Grotzinger et al., 2012). The ChemCam instrument suite, which employs laser-induced  
51 breakdown spectroscopy (LIBS) to measure the elemental composition of a Martian target at  
52 stand-off distances between 1.3 m and 7 m from the rover (Maurice et al., 2012), has acquired  
53 more than 188,000 spectra from over 650 Martian targets during its nominal mission alone  
54 (Maurice et al., 2016), and has since surpassed 500,000 laser shots. Three spectrometers allow  
55 spectral measurements from 242 nm to 900 nm, with gaps at 335-385 nm and at 465-510 nm  
56 (Wiens et al., 2012). A camera known as the Remote Micro-Imager provides visual context for  
57 the measured spectra, and is also used to autofocus the laser on the target after the malfunction of  
58 the focusing laser on sol 801 (Peret et al., 2016). Following the ongoing success of the  
59 ChemCam instrument, an enhanced follow-up instrument called SuperCam is planned for the  
60 upcoming Mars 2020 mission (Maurice et al., 2015; Wiens et al., 2016). Like its predecessor,

61 SuperCam will employ LIBS among other spectroscopic methods (Raman spectroscopy, visible  
62 and near infrared spectroscopy, and time-resolved fluorescence spectroscopy) to analyze the  
63 elemental and mineralogical composition of Martian targets.

64 LIBS is a kind of atomic emission spectroscopy that uses a high-intensity laser pulse to form a  
65 plasma from ablated sample material (e.g. Cremers and Radziemski, 2006). The plasma consists  
66 of atoms, ions, electrons, and simple molecules. Electrons emit a continuum due to  
67 bremsstrahlung and recombination events, while radiative transitions from atoms, ions, and  
68 simple molecules result in characteristic emission lines and bands in the spectrum. Analysis of  
69 these emissions reveals the elemental composition of the sample. LIBS is well suited for remote  
70 sensing in extraterrestrial exploration, as it requires no sample preparation and can be performed  
71 over distances of several meters (Knight et al., 2000). The technique can be used in a wide range  
72 of environments, from vacuum to high-pressure conditions like those found on the surface of  
73 Venus (Arp et al., 2004). The atmospheric pressure of around 7 hPa on Mars is near-optimal for  
74 LIBS, however, as it confines the plasma plume moderately while reducing the collision  
75 frequency, resulting in a high signal intensity (Knight et al., 2000).

76 The emission spectrum of an element depends on the distribution of its electronic energy  
77 levels. Halogens such as chlorine have very high excited electronic energy levels, so that the  
78 strongest emission lines are in the ultraviolet (UV), where common LIBS set-ups are not  
79 sensitive (Cremers and Radziemski, 1983). Emission lines in the visible and near-infrared  
80 spectral range, such as the neutral Cl line at 837.6 nm, are low in intensity. The detection of  
81 chlorine with ChemCam has therefore been challenging (Anderson et al., 2017), and the presence  
82 of chlorides in Martian targets can sometimes only be inferred from strong emissions by a likely  
83 cation (e.g. Clegg et al., 2013).

84 Recently, it has been shown that LIBS sensitivity for halogens can be significantly improved  
85 by using molecular emission from the simple molecules that form as the halogens recombine in  
86 the plasma (Gaft et al., 2014). Emission spectra of these molecules consist of more or less  
87 intense bands with characteristic shapes that can often be easily identified and are well-  
88 documented (e.g. Pearse and Gaydon, 1976). The observation of molecular bands of calcium  
89 monofluoride (CaF) in ChemCam spectra allowed for the detection of fluorine for the first time  
90 on Mars (Forni et al., 2015). Likewise, indirect detection of chlorine via calcium monochloride  
91 (CaCl) bands has improved the detection of chlorine in Martian samples (Cousin et al., 2015;

92 Forni et al., 2015). The most intense CaCl bands are the orange system ( $B^2\Sigma - X^2\Sigma$ , short “B–  
93 X band”) from 581 nm to 607 nm, and the red system ( $A^2\Pi - X^2\Sigma$ , short “A–X band”) from  
94 605 nm to 636 nm (Pearse and Gaydon, 1976). Both are well within the third wavelength range  
95 of ChemCam.

96 A prerequisite for the analysis of CaCl bands is that both Ca and Cl are present in sufficient  
97 amounts in the plasma. The calcium that is necessary to form CaCl can be supplied by minerals  
98 such as feldspar ( $KAlSi_3O_8 - NaAlSi_3O_8 - CaAl_2Si_2O_8$ ) or calcium sulfate ( $CaSO_4$ ), which have  
99 been found in Martian soil and rocks (Bish et al., 2013; Ehlmann et al., 2011; Meslin et al., 2013).  
100 However, the relation between the relative concentrations of Ca and Cl and the intensity of the  
101 CaCl bands under Martian conditions is still unclear. For example, various ChemCam spectra  
102 have shown strong signals from Ca and Cl, even though no CaCl bands have been detected  
103 (Cousin et al., 2015). In order to understand these observations and to help with the interpretation  
104 of Martian LIBS data, it is important to investigate the conditions which favor the formation of  
105 CaCl.

106 The high intensity of the CaCl bands makes them well suited for the indirect detection of  
107 chlorine, but they are not the only molecular bands that are available. Chlorine can also  
108 recombine into other molecules, especially if alkaline earth metals are present. Magnesium is of  
109 special interest in this regard due to its occurrence on Mars, where it has been found in water-  
110 related materials such as sulfates, chlorides, and perchlorates (Ehlmann and Edwards, 2014). It is  
111 therefore important to investigate whether chlorine could be indirectly detected by MgCl  
112 emission in LIBS spectra. It might also be possible that the formation of MgCl is preferred over  
113 the formation of CaCl (Maurice et al., 2016). In this case, the intensity of CaCl bands would be  
114 reduced if Mg is present, which would significantly limit the detection of chlorine by CaCl  
115 emission in Martian spectra. It is not possible to observe the strongest MgCl band with  
116 ChemCam or SuperCam, as it is located between 375 nm and 378 nm, where these instruments  
117 have a gap in their spectral coverage.

118 In this study, CaCl bands in LIBS spectra measured in simulated Martian atmospheric  
119 conditions are analyzed to investigate their characteristics and dependencies with varying  
120 concentrations of Ca and Cl and to evaluate the suitability of CaCl emission for quantitative  
121 analysis of chlorine on Mars. The samples are mixtures of chloride salts, sulfate minerals and  
122 Martian regolith simulant. The chlorides and sulfates used here have already been detected on

123 Mars and are of high interest in the context of the search for water on Mars. The intensity of the  
124 CaCl bands in these samples is investigated in dependence of the Ca and Cl content of the  
125 samples and for different measurement times. A model is developed to simulate the reaction  
126 kinetics inside the plasma and to reveal the critical parameters affecting the intensity of the CaCl  
127 bands. Additionally, the MgCl band is investigated in order to determine its suitability for the  
128 indirect analysis of chlorine, and to find out whether the presence of Mg has an effect on the  
129 CaCl emission intensity.

## 130 **2. Methods**

### 131 *2.1. Sample preparation*

132 In this study, pure and mixed samples of six salts (MgCl<sub>2</sub>, CaCl<sub>2</sub>, NaCl, KCl, MgSO<sub>4</sub>, CaSO<sub>4</sub>),  
133 Martian regolith simulant JSC Mars-1A (“JSC”), and a dunite reference material are investigated.  
134 The salts were selected because they are of high interest in the context of brine formation on  
135 Mars (Möhlmann and Thomsen, 2011; Schröder et al., 2013). An overview of the samples is  
136 given in Table 1.

137 A pure sample of the hexahydrate of magnesium chloride (MgCl<sub>2</sub> · 6 H<sub>2</sub>O) was made for the  
138 investigation of the MgCl band. The dihydrate of calcium chloride (CaCl<sub>2</sub> · 2 H<sub>2</sub>O) as well as  
139 potassium chloride (KCl) and sodium chloride (NaCl) were used for the investigation of the  
140 CaCl bands. In order to produce samples with varying concentrations of Cl and Ca, mixtures of  
141 these chlorides with sulfate minerals and with JSC were made at different weight ratios. The  
142 sulfate mineral used for mixtures with CaCl<sub>2</sub> was the heptahydrate of magnesium sulfate  
143 (MgSO<sub>4</sub> · 7 H<sub>2</sub>O). For mixtures with KCl and NaCl, the dihydrate of calcium sulfate  
144 (CaSO<sub>4</sub> · 2 H<sub>2</sub>O) was used, which supplies the calcium for the possible formation of CaCl inside  
145 the plasma. In mixtures with JSC, the calcium is provided by the feldspar in JSC, which  
146 contributes the equivalent of about 6.2 wt% CaO to the chemical composition of JSC (Allen et  
147 al., 1998). The concentrations of Ca and Cl are correlated in mixtures with CaCl<sub>2</sub>, and anti-  
148 correlated in mixtures with NaCl and KCl. Reagent-grade salts were used for the samples.

149 The substances were mixed and ground into powders with a typical grain size of less than  
150 40 µm, which were then pressed into pellets of about 1 g, using a pressure of 5 tons for  
151 10 minutes. Due to the hygroscopic nature of MgSO<sub>4</sub>, MgCl<sub>2</sub>, and CaCl<sub>2</sub>, samples containing

152 these substances were stored inside a desiccator in order to minimize the adsorption of  
153 atmospheric water.

154

Table 1: Overview of samples investigated in this study

Sample/mixture	Composition
CaCl <sub>2</sub>	100 wt%
MgCl <sub>2</sub>	100 wt%
Dunite (CRM 4233-88)	100 wt%
JSC	100 wt%
CaSO <sub>4</sub>	100 wt%
CaCl <sub>2</sub> + MgSO <sub>4</sub>	0.2 wt% to 80 wt% CaCl <sub>2</sub> (17 samples)
KCl + CaSO <sub>4</sub>	0.5 wt% to 80 wt% KCl (14 samples)
NaCl + CaSO <sub>4</sub>	1 wt% to 80 wt% NaCl (11 samples)
CaCl <sub>2</sub> + JSC	1 wt% to 24 wt% CaCl <sub>2</sub> (7 samples)
KCl + JSC	1.2 wt% to 17 wt% KCl (9 samples)
NaCl + JSC	5 wt% to 60 wt% NaCl (8 samples)

155

## 156 2.2. Experimental setup

157 Measurements were made with the LIBS system at Deutsches Zentrum für Luft- und  
158 Raumfahrt (DLR). The laser is a Q-switched Nd:YAG laser with a wavelength of 1064 nm and a  
159 pulse length of 8 ns. It was operated at a repetition rate of 10 Hz. The maximum laser energy of  
160 51 mJ/pulse (measured at the sample position) was reduced to 22 mJ/pulse with gray filters in the  
161 optical path. The samples were placed inside a vacuum chamber filled with Mars-analog  
162 atmosphere consisting of 95.55 vol% CO<sub>2</sub>, 2.7 vol% N<sub>2</sub>, 1.6 vol% Ar, and 0.15 vol% O<sub>2</sub>. The  
163 pressure inside the chamber was kept constant at 6.5 hPa.

164 The plasma emission was measured with an echelle spectrometer (LTB Aryelle Butterfly),  
165 which uses a time-gated intensified charge-coupled device (ICCD) camera (Andor iStar). The  
166 spectra cover a wavelength range from 270 nm to 850 nm, with a pixel resolution of 11 pm at  
167 270 nm and 34 pm at 850 nm.

168 Each sample was measured at multiple positions in order to obtain a good representation of  
169 the sample composition. At each position, the intensity values of the plasma emissions of 30  
170 successive laser shots were summed up to obtain a single spectrum. Measurements of mixtures

171 of  $\text{CaCl}_2$  and  $\text{MgSO}_4$  were made using three positions per sample for each setting of delay time  
172 and integration time. Because of the relatively high uncertainty values of the signals in these  
173 measurements, the decision was made to increase the number of positions from three to ten  
174 positions for the remaining samples.

### 175 *2.3. Data acquisition and processing*

176 In the early stages of the plasma evolution, radiative recombination and bremsstrahlung lead  
177 to a strong continuum emission, which can obscure the signals from molecular bands. Baseline  
178 removal algorithms can be used to remove the continuum retroactively from the recorded  
179 spectrum. However, these algorithms can remove molecular bands as well, since molecular  
180 bands cover a wide wavelength range (about 10 nm for the A-X band of CaCl) and cannot be  
181 separated from the baseline as easily as atomic or ionic emission lines. In echelle spectra, the  
182 removal of the baseline is further complicated by the fact that the apparatus function is not  
183 smooth. The total spectrum is combined from successive orders, in which the sensitivity  
184 decreases as the distance to the central wavelength (blaze angle) increases, resulting in a baseline  
185 that is not smooth at the transition between adjacent orders. As most baseline removal algorithms  
186 require a smooth baseline in order to work as intended, an additional step would be necessary in  
187 which the sensitivity of the spectrometer is normalized before removing the baseline. This is  
188 often not desirable, as each of these steps introduces new uncertainties.

189 A simple and common approach is to gate out the continuous emission during the experiment  
190 instead. This can be achieved with an ICCD, for example, by setting a delay time between the  
191 laser pulse and the start of the measurement. As the plasma expands and cools off, the continuum  
192 emission drops off quickly within several hundred nanoseconds, so that it will not appear in  
193 spectra with a delay time larger than that. Molecular bands produce a strong signal that can still  
194 be detected microseconds after plasma initiation, so that their signal benefits from long  
195 integration times. The delay time and the integration time are defining parameters of the LIBS  
196 measurement and have to be adjusted with regard to the measurement objective, the setup, and  
197 the samples.

198 Different combinations of delay time and integration time were analyzed using pure  $\text{CaCl}_2$   
199 samples in order to find optimal parameters for the observation of CaCl bands with our setup.  
200 Based on the comparison of the signal intensities of the A-X band of CaCl and the continuum  
201 emission (see Section 3.3), a delay time of 350 ns and an integration time of 10  $\mu\text{s}$  were selected

202 and were used to measure spectra of all mixed samples. Additionally, the samples were measured  
203 with parameters similar to those used by ChemCam, with the delay time set to zero and an  
204 integration time of 3 ms. In order to correctly measure the intensities of emission lines and  
205 molecular bands, the continuum emission was retroactively removed from all measurements with  
206 a delay time of less than 150 ns. This was done using a custom baseline fit that multiplies a  
207 polynomial for the continuum emission with blaze functions for the orders of the echelle  
208 spectrometer.

209 Signals from emission lines and molecular bands were measured by taking the average  
210 intensity count in a specified wavelength range for each spectrum (Table 2). Mean value and  
211 standard deviation were then calculated from the emission intensities that were obtained at  
212 different positions on the sample.

213

Table 2: Spectral emissions and associated wavelength ranges used for the calculation of signal intensities in this study

Emission	Wavelength range
Ca I	422.3 – 423.0 nm
CaCl ( $A^2\Pi - X^2\Sigma$ )	620.4 – 621.0 nm
Continuum	637.0 – 639.0 nm

214

### 215 **3. Experimental Results**

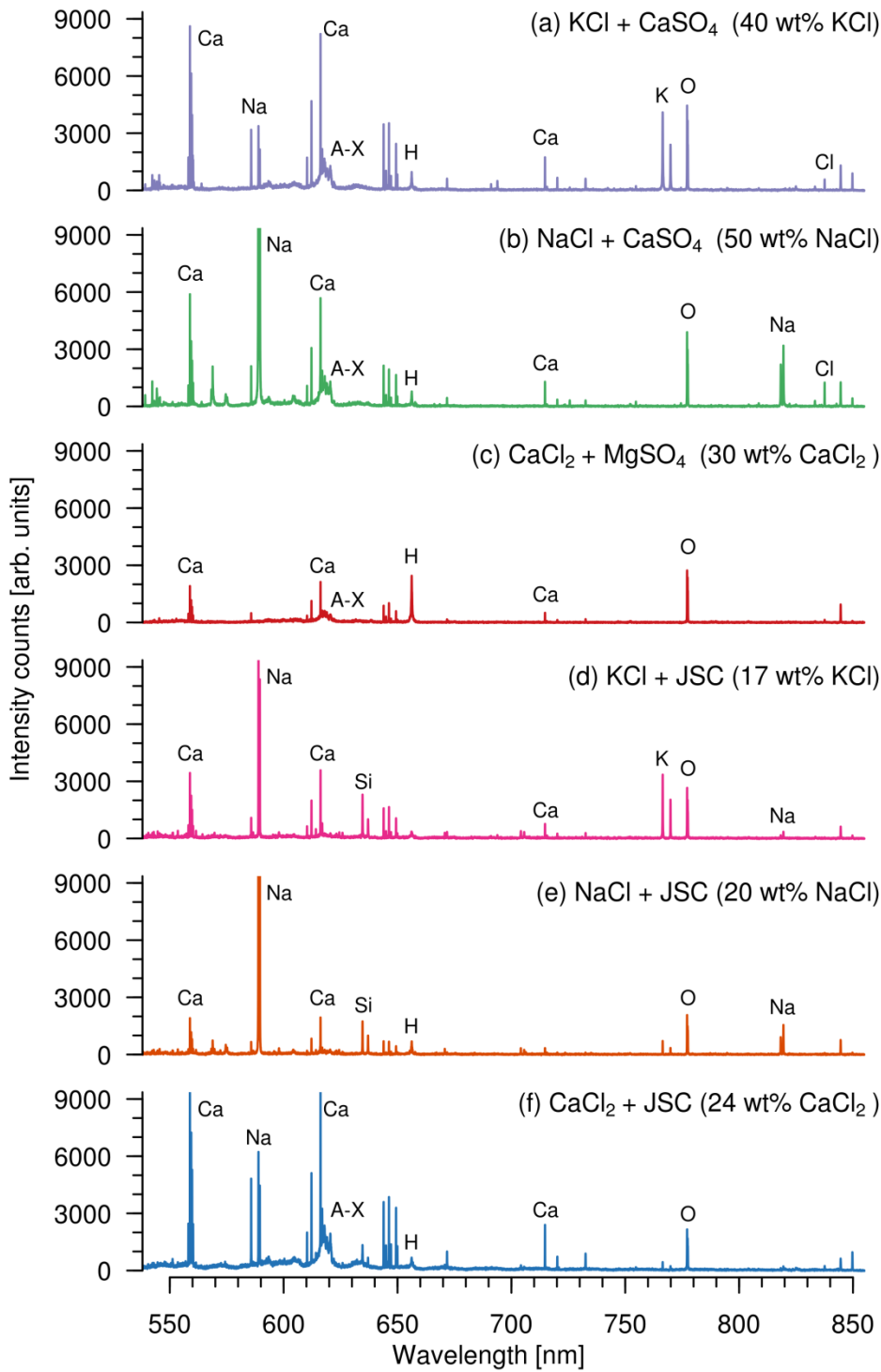
#### 216 *3.1. LIBS spectra and general characteristics*

217 In order to illustrate the measurements that were made, exemplary spectra of all mixtures are  
218 shown in Fig. 1, with labels for some of the stronger emission lines and for the A–X band. The  
219 Cl line at 837.6 nm can be clearly seen for the samples of KCl mixed with CaSO<sub>4</sub> and of NaCl  
220 mixed with CaSO<sub>4</sub> (Fig. 1a and b), which have the highest chlorine content of the shown spectra.  
221 As expected, the Cl line is less intense than the emission lines of both K and Na, which are  
222 present in equal concentrations as Cl in their respective samples. In contrast to the low intensity  
223 of the Cl line, there is a strong signal from the A–X band in many of the spectra, even when the  
224 Cl line cannot be observed.

225 The spectrum of  $\text{CaCl}_2$  mixed with  $\text{MgSO}_4$  shows a strong hydrogen emission (Fig. 1c). This  
226 indicates that, although samples containing these salts were stored in a desiccator, the hydration  
227 state was still high at the time of measurement. During the measurements, the formation of liquid  
228 water on the surface of the pellets could be observed, which further hints at strong adsorption of  
229 atmospheric water. The low total intensity of the spectrum is most likely related to the high  
230 translucence caused by the hydration and adsorption of water, as a high translucence reduces the  
231 coupling efficiency of the laser (Schröder et al., 2013). In the spectra of  $\text{KCl}$  and  $\text{NaCl}$  mixed  
232 with JSC (Fig. 1d and e), the H line is less intense, indicating that the samples were drier. Intense  
233 Ca emission lines can be observed in these samples, as JSC contains the equivalent of about  
234 6.2 wt%  $\text{CaO}$  (Allen et al., 1998). For a mixture of 24 wt%  $\text{CaCl}_2$  and 76 wt% JSC (Fig. 1f), Ca  
235 emissions are twice as strong as for pure JSC. This is in agreement with the chemical  
236 composition of JSC, according to which pure JSC should contain about 25,600 ppm of Ca, while  
237 a mixture with 24 wt%  $\text{CaCl}_2$  should contain about 50,400 ppm of Ca. This concentration of Ca  
238 in JSC should be sufficient to allow for the observation of  $\text{CaCl}$  bands even in mixtures with  
239 calcium-free chlorides. Indeed, the distinct shape of the A–X band can be recognized in Fig. 1d  
240 and e, if the corresponding parts of the spectra are magnified.

241 In Fig. 2, spectra of mixed samples of  $\text{CaCl}_2$  and JSC are shown which focus on the  
242 wavelength range of the B–X band and the A–X band of  $\text{CaCl}$ . As expected, the band intensities  
243 get stronger with increasing  $\text{CaCl}_2$  content in the sample. Three band sequences can be observed  
244 in the A–X band, while individual heads can be observed in the B–X band. The B–X band is of  
245 much lower intensity than the A–X band. While a lower intensity is to be expected for the B–X  
246 band (Pearse and Gaydon, 1976), the intensity is further reduced because the band is at the  
247 transition of two adjacent echelle orders, where the sensitivity of the spectrometer is up to 45%  
248 lower than it is at the center of an order. As the A-X band shows an improved signal-to-noise  
249 ratio in comparison to the B-X band, the decision was made to focus on the A–X band for this  
250 study. The location of the A–X band at the center of an echelle order allows for detection with  
251 high sensitivity and an easy separation from the continuum emission.

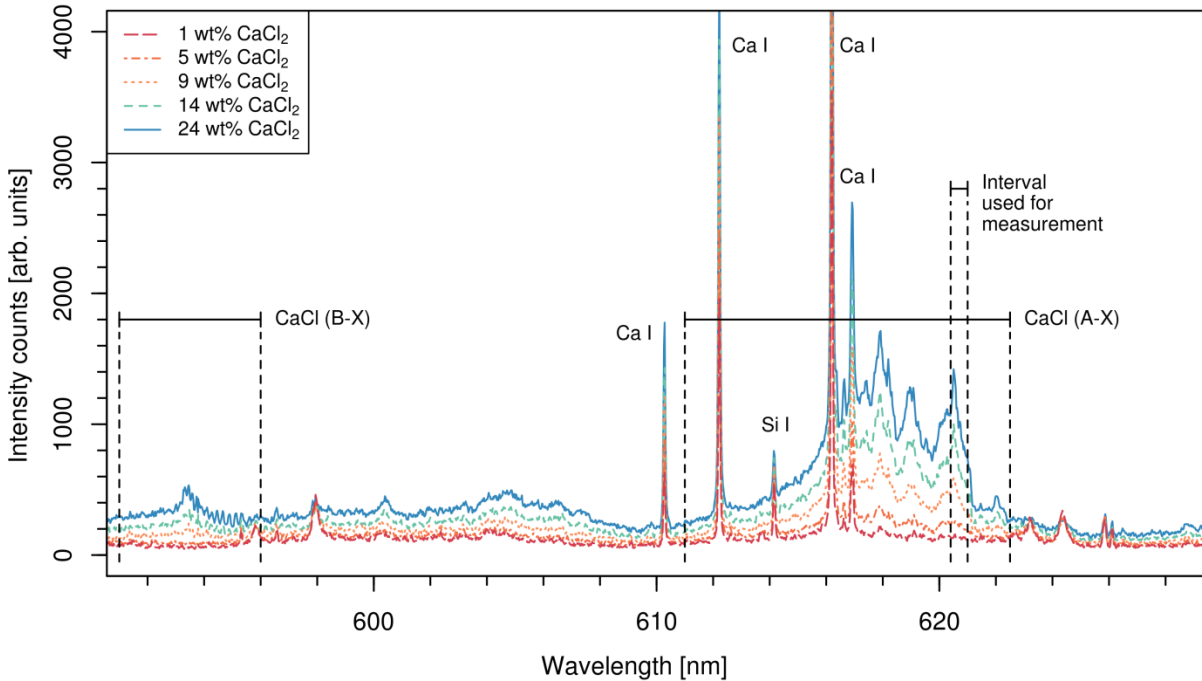
252



253

Figure 1: Spectra representing all mixed samples, with labels for important emission lines and for the A–X band of CaCl. Despite careful sample preparation, weak Na lines can be observed in (a). This hints at a (very low) contamination, most likely with NaCl.

254



255

Figure 2: Spectra of JSC mixed with different amounts of  $\text{CaCl}_2$ . The A–X band (from about 611 nm to 622.5 nm) can be seen easily, while the B–X band (from about 591 nm to 596 nm) is less intense due to the echelle spectrometer’s reduced sensitivity in this spectral range.

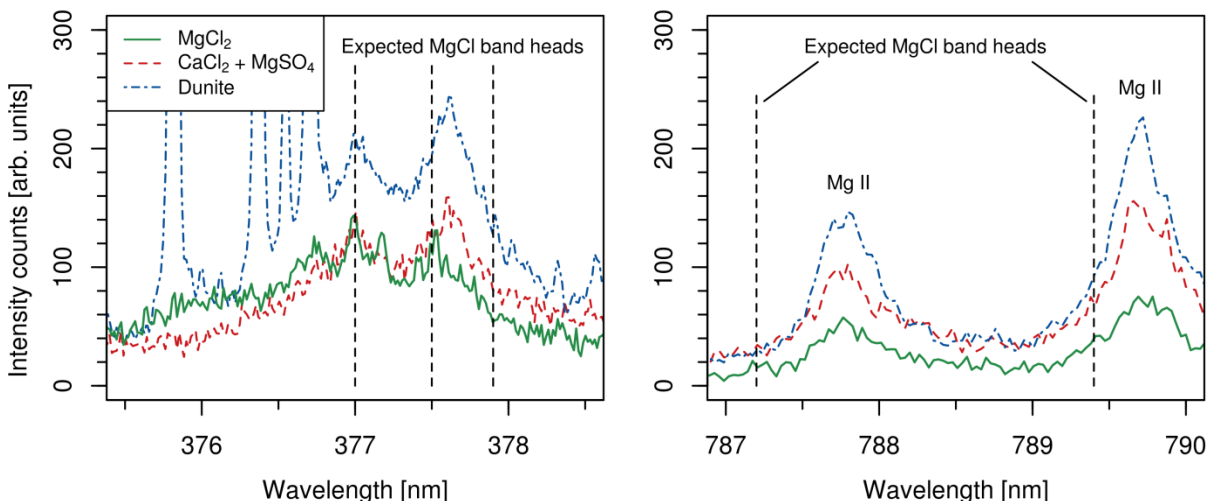
256

### 257 3.2. Comparison of $\text{MgCl}$ and $\text{CaCl}$ bands

258 Fig. 3 shows spectra of pure  $\text{MgCl}_2$  and of the dunite reference sample, which contains the  
 259 equivalent of 41.86 wt%  $\text{MgO}$ , but does not contain chlorine. The strongest  $\text{MgCl}$  band is  
 260 expected to exhibit strong heads at 377 nm, 377.5 nm, and 377.9 nm (Pearse and Gaydon, 1976).  
 261 Another  $\text{MgCl}$  band with heads at 787.2 nm and 789.4 nm has also been reported (Querbach,  
 262 1930).

263 Weak band structures can be observed between 376 nm and 379 nm. However, the observed  
 264 band heads do not match the reported positions of the  $\text{MgCl}$  band heads, with the exception of  
 265 the head at 377 nm. In the measured spectra, there is a head at about 377.5 nm that is  
 266 unaccounted for in the literature, while the other reported heads cannot be observed at all. Most  
 267 importantly, the band structures between 376 nm and 379 nm can also be observed in the  
 268 spectrum of the dunite sample. This strongly indicates that these signals are not caused by  
 269 molecular emissions of  $\text{MgCl}$ . As they have not been observed in samples that did not contain

270 magnesium, it is most likely that they are based on emissions of MgO, MgOH, or more complex  
271 polyatomic molecules containing magnesium. Potential heads of MgCl emissions cannot be  
272 distinguished from these superimposed band structures.



273  
274  
275 Figure 3: Spectra of pure MgCl<sub>2</sub>, a sample of 9 wt% CaCl<sub>2</sub> and 91 wt% MgSO<sub>4</sub>, and the dunite reference material. The observed signals around 377 nm are not the expected MgCl bands, since they are also present in the dunite sample, which contains no chlorine. It is unclear which molecules are responsible for the observed molecular bands. Between 787 nm and 790 nm, no molecular bands can be observed for any of the investigated samples.

276  
277  
278  
279  
280  
281  
282  
283  
284  
285  
286  
287

### 3.3. Variation of delay time for CaCl<sub>2</sub>

Fig. 4a shows the intensities of the A–X band and of the continuum emission at different delay times in samples of pure CaCl<sub>2</sub>. The integration time was kept constant at 500 ns. The continuum emission declines quickly and does not significantly contribute to the intensity of the spectrum for delay times larger than 250 ns. The CaCl band, on the other hand, reaches its highest intensity after 1 μs and decreases slowly over time, so that a clear signal can still be detected even with a delay time of 5 μs. The long delay between the formation of the plasma plume and the maximum intensity of the CaCl band can be explained by the time it takes for Ca and Cl to recombine into CaCl. The reaction kinetics model used to fit the CaCl band follows the evolution of the band intensity closely, and will be discussed in more detail in Section 4. Fig. 4b shows the temporal change in CaCl concentration as calculated from the fit model. The intensity of the continuum (Fig. 4a) was fitted by the sum of two exponential functions, in accordance with a continuum that is dominated by bremsstrahlung in the early stages and dominated by

288 radiative recombination in the later stages of the cooling plasma (D'Ammando et al., 2010; De  
289 Giacomo et al., 2010).

290 A delay time bigger than 250 ns minimizes the contribution of the continuum to the band  
291 signal intensity, while a delay time of less than 1  $\mu$ s helps to increase the intensity of the CaCl  
292 band. Based on these results, a delay time of 350 ns was set in one of the two measurement  
293 settings for the analysis of the CaCl band intensity in mixed samples. The choice of integration  
294 time depends on the intended analysis. Shorter integration times will result in more accurate  
295 snapshots of the molecular bands at a certain time after plasma initiation, while long integration  
296 times will yield stronger signals, which allow the detection of smaller quantities of chlorine. As  
297 integration times longer than 10  $\mu$ s did not significantly improve the CaCl band intensity in  
298 measurements of pure CaCl<sub>2</sub>, the integration time for measurements with a delay time of 350 ns  
299 was set to 10  $\mu$ s.

300 The plasma temperature  $T$  was calculated for all delay times from individual Saha-Boltzmann  
301 plots (e.g. Aragón and Aguilera, 2008) of the most persistent Ca lines and Cl lines (Table 3) as  
302 seen in Fig. 5a. Fig. 5b shows the temporal evolution of the plasma temperatures. The decrease  
303 from initial temperature  $T_0$  was modeled using Newton's law of cooling with the saturation  
304 temperature  $T_{Sat}$  and the cooling rate constant  $C_T$ :

$$T(t) = (T_0 - T_{Sat}) \exp(-C_T t) + T_{Sat} \quad (1)$$

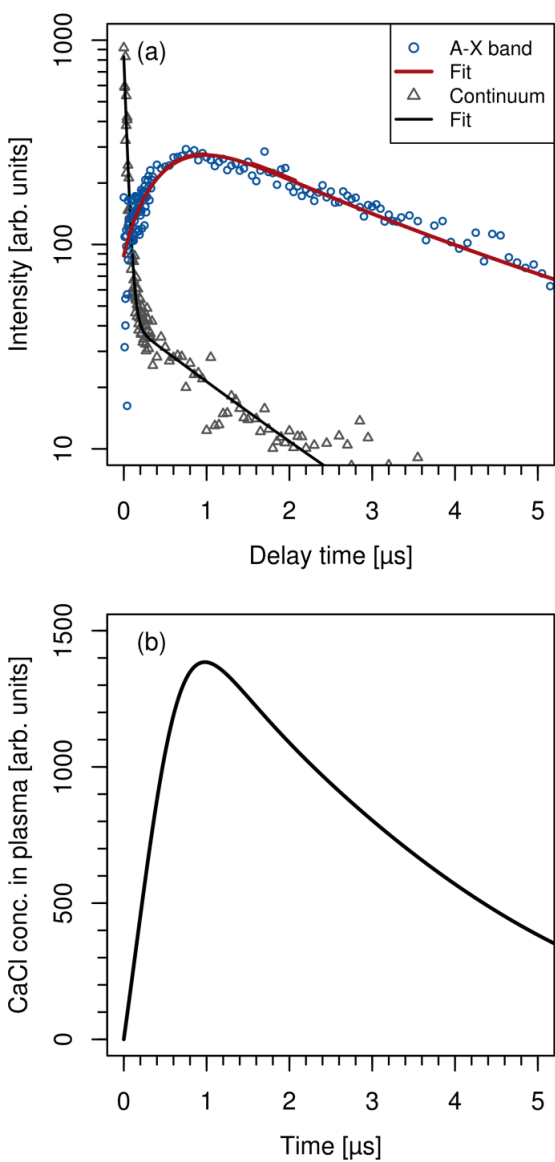
306  
307 In order to fit the temperature values from the Saha-Boltzmann plots, the integral of (1) over  
308 the gate time was used. The resulting fit parameters for Ca lines and Cl lines are shown in Table  
309 4.

310 The saturation temperatures are reached after about 4  $\mu$ s and differ by almost 8000 K. The  
311 temperature calculated from Cl lines is higher than the temperature calculated from Ca lines.  
312 This might be an indication of a spatial separation of the species inside the plasma. Differences  
313 in the density distributions and expansion of the elements in LIBS plasma plumes have been  
314 reported in various publications (e.g. Aguilera et al., 2003; De Giacomo et al., 2008; Lee et al.,  
315 1992). Since the temperature is higher in the center of the plasma plume (Aguilera et al., 2003),  
316 the differences in the measured temperatures could be explained by different density

317 distributions for Cl and Ca, where Cl atoms and ions are generally closer to the center of the  
318 plasma. In this case, reactions will only take place in an overlapping region.

319 A very similar difference between temperatures calculated from Ca lines and from Cl lines  
320 can be observed for the mixed samples (Fig. 5c). The magnitude of the temperature stays  
321 approximately the same for all samples, although the temperatures seem to be slightly higher in  
322 JSC mixtures. It is worth noting, however, that the requirements for local thermodynamic  
323 equilibrium are not met in these measurements. Due to the long integration time, a small  
324 variation of electron number density and temperature cannot be assumed, even if the McWhirter  
325 criterion holds (Cristoforetti et al., 2010). Therefore, a high uncertainty is associated with these  
326 values and only qualitative observations can be made.

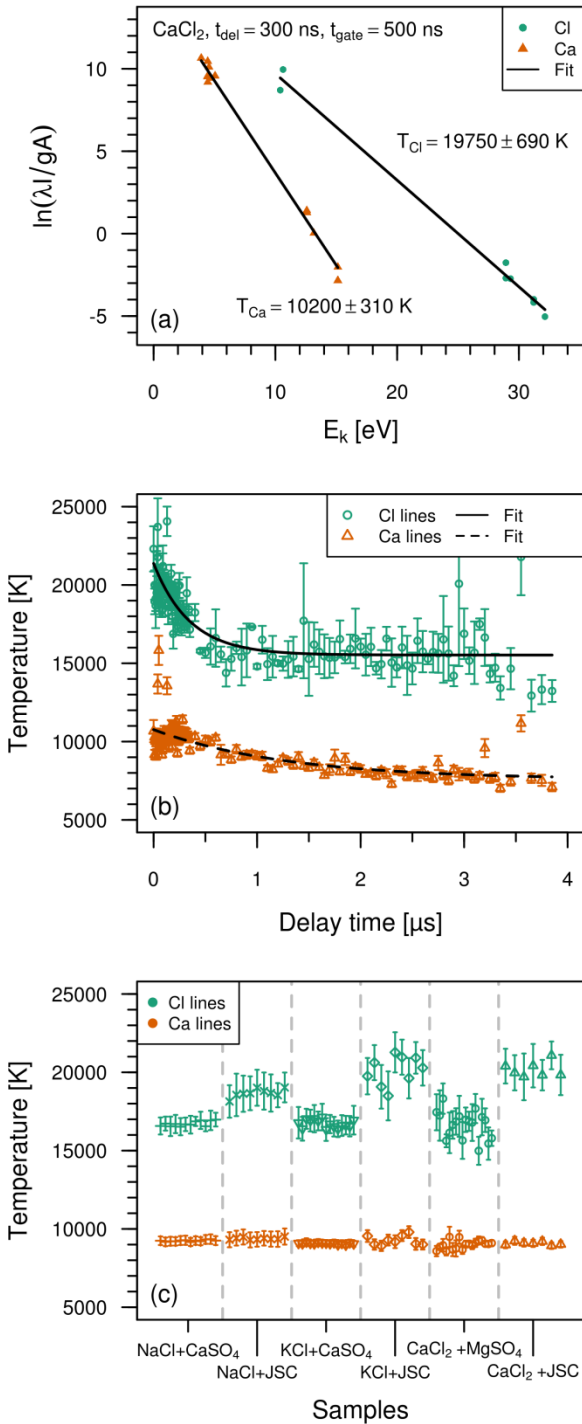
327



328

Figure 4: (a) A–X band of CaCl and continuum emission for different delay times, with constant integration times of 500 ns. The temporal evolution of the CaCl band was fitted using the reaction kinetics model (see Section 4), while the continuum was fitted by the sum of two exponential functions, indicating two separate time regimes for the continuum. (b) Calculated temporal evolution of the CaCl concentration in the plasma of  $\text{CaCl}_2$  based on the fit seen in (a). The highest CaCl concentration is reached after about 1  $\mu\text{s}$ , then it drops slowly.

329



330

Figure 5: (a) Saha-Boltzmann plots of Ca and Cl from a measurement of pure  $\text{CaCl}_2$  with a gate delay of 300 ns and an integration time of 500 ns. The temperature can be calculated from the slope of the fit. (b) Temperature values for pure  $\text{CaCl}_2$  at varying gate delay times, with the integration time set to 500 ns. (c) Temperature values for all mixed samples, measured with a gate delay of 350 ns and an integration time of 10  $\mu\text{s}$ . The temperatures calculated from Cl lines are significantly higher than the temperatures calculated from Ca lines.

Table 3: Emission lines used for the temperature calculation using Saha-Boltzmann plots (data from the NIST Atomic Spectra Database).

Emission	Wavelength (nm)	$gA$ ( $10^8/s$ )	$E_k$ (eV)	Emission	Wavelength (nm)	$gA$ ( $10^8/s$ )	$E_k$ (eV)
Ca I	445.48	6.1	4.68	Cl I	754.71	0.48	10.63
Ca I	585.75	3.3	5.05	Cl I	837.59	2.2	10.40
Ca I	616.22	1.43	3.91	Cl II	386.08	24	19.17
Ca I	643.91	4.8	4.45	Cl II	479.46	7.28	15.96
Ca I	644.98	0.45	4.44	Cl II	489.68	7.9	18.25
Ca I	646.26	3.3	4.44	Cl II	490.48	5.7	18.24
Ca I	649.38	2.2	4.43	Cl II	521.79	3.9	16.34
Ca I	671.77	0.36	4.55	Cl II	542.32	1.3	15.96
Ca II	315.89	12	7.05				
Ca II	370.60	1.8	6.47				
Ca II	373.69	3.4	6.47				
Ca II	820.17	2	9.02				
Ca II	824.88	3.7	9.02				

Table 4: Parameters of the temperature fit

Parameter	Ca lines	Cl lines
$T_0$	$(11.9 \pm 0.5) \times 10^3$ K	$(32 \pm 4) \times 10^3$ K
$T_{Sat}$	$(7.6 \pm 0.4) \times 10^3$ K	$(15.5 \pm 0.3) \times 10^3$ K
$C_T$	$(0.8 \pm 0.3) \times 10^6$ s <sup>-1</sup>	$(2.8 \pm 0.5) \times 10^6$ s <sup>-1</sup>

332

### 333 3.4. Variation of Cl and Ca concentration

334 The primary goal of the investigation of mixed samples was to find the ratio of Ca to Cl that  
 335 leads to the strongest CaCl band signal, and to find out whether the CaCl band signal scales  
 336 linearly with Cl concentration. The concentrations of Ca and Cl are correlated in mixtures of  
 337 CaCl<sub>2</sub> with MgSO<sub>4</sub> or JSC, and anti-correlated in mixtures of NaCl or KCl with CaSO<sub>4</sub> or JSC.

338 Fig. 6 shows the intensity of the A–X band for all samples, measured with a delay time of  
 339 350 ns and an integration time of 10  $\mu$ s, and without a delay with an integration time of 3 ms. As  
 340 expected, the highest band intensities are reached for compositions that are high in both Ca and  
 341 Cl content. In samples where Ca and Cl are anti-correlated (Fig. 6a-d), this is the case for a Cl

342 concentration of between  $1 \times 10^5$  ppm and  $2 \times 10^5$  ppm, which corresponds to about  $0.7 \times 10^5$  ppm  
343 to  $0.5 \times 10^5$  ppm of Ca. The exact concentrations of the maximum intensity depend not only on  
344 the sample composition, but also on the choice of the measurement time. After quickly reaching  
345 the maximum at comparatively low Cl concentrations, the band intensity slowly declines as the  
346 concentration of Cl increases and that of Ca decreases in the sample. This asymmetry suggests  
347 that a high Ca content is more important for the formation of CaCl than a high Cl content.

348 The overall highest band intensities are reached in samples with a high content of CaCl<sub>2</sub>,  
349 which provides both reactants (Fig. 6e, f). However, for low chlorine concentrations below  
350 60,000 ppm, mixtures of NaCl and KCl with CaSO<sub>4</sub> reach higher intensities than mixtures with  
351 CaCl<sub>2</sub> due to the high amount of Ca supplied by the CaSO<sub>4</sub>, which leads to an increased reaction  
352 rate. For NaCl or KCl mixed with JSC (Fig. 6b, d), the A–X band intensities are relatively low,  
353 so that they can only be used to detect Cl at high concentrations, where they might be surpassed  
354 in intensity by the atomic Cl lines.

355 The low CaCl band intensity in samples of NaCl or KCl mixed with JSC can be explained by  
356 the relatively low amount of Ca in JSC (about 25,000 ppm). However, the spectra still show  
357 strong Ca lines even in samples with a low JSC content. In these samples, Cl lines can also be  
358 observed, which surpass the intensity of the CaCl band. This can result in spectra that have  
359 strong atomic lines from Ca and Cl, but only have weak CaCl bands. If the plasma intensity is  
360 weak, and the spectrometer has a low resolution, then the CaCl band might not be observed at all.  
361 This has to be considered for ChemCam and SuperCam, as it means that it is possible to observe  
362 atomic lines from both Ca and Cl in Martian targets, without necessarily also detecting a CaCl  
363 band signal.

364 Due to the dependency of the CaCl signal on the concentrations of both Ca and Cl in the  
365 sample, it is not possible to calculate the Cl concentration directly from the intensity of the CaCl  
366 band. However, the composition of an unknown target can still be qualitatively estimated by  
367 comparing the intensity of the CaCl band to that of the emissions of Ca, Na, K, and other  
368 potential cations of chloride salts. This is illustrated in Fig. 7, which shows the intensity of  
369 atomic emission lines of Ca, Cl, K, and Na over the CaCl band intensity for all mixed samples. If  
370 the Ca line, the Cl line and the CaCl band are very intense, then the target likely contains high  
371 amounts of CaCl<sub>2</sub>, since high band intensities can only be reached if there is an abundance of  
372 both Ca and Cl. If there is a strong signal from the Ca line, but a weak signal from the CaCl band,

373 then the chlorine is most likely supplied by a calcium-free salt in low concentration. In this case,  
374 emissions from the corresponding cation can be observed. Therefore, the CaCl band can be used  
375 in conjunction with other signals in the spectrum to make a qualitative assessment of the target.  
376 In simple cases, where the chloride-bearing salts can be clearly identified, a quantification of the  
377 Cl concentration is not necessary anymore, as it is sufficient to quantify the concentration of the  
378 cation. For more complex cases, a multivariate approach is required. Multivariate data analysis  
379 takes all the interdependencies into account which determine the signal intensities of CaCl, Ca,  
380 Cl, and the potential cations of the chloride salts. As a result, the quantification of chlorine via  
381 molecular emission is an ideal case for a multivariate approach and should be possible even for  
382 complex compositions.

383

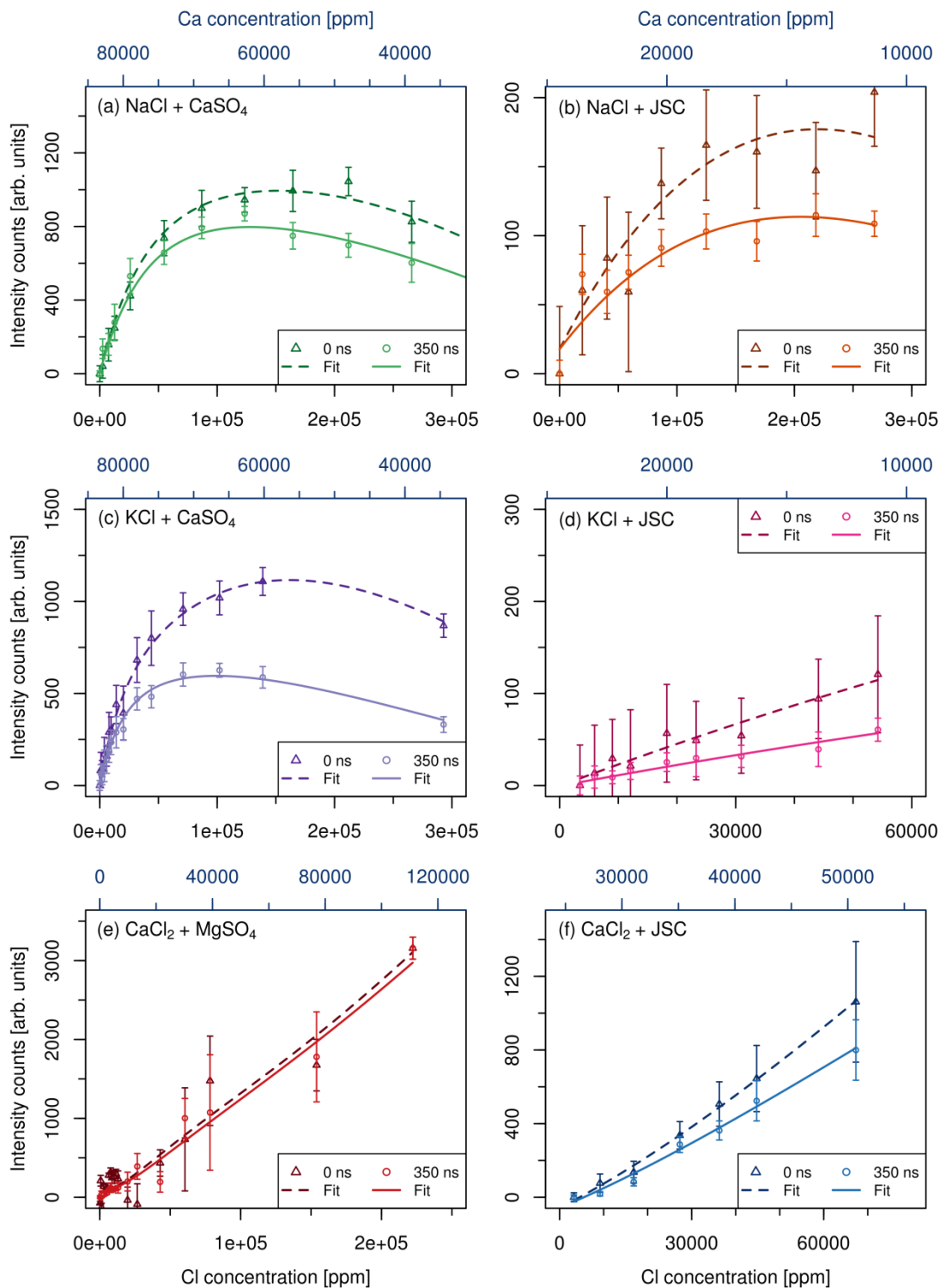
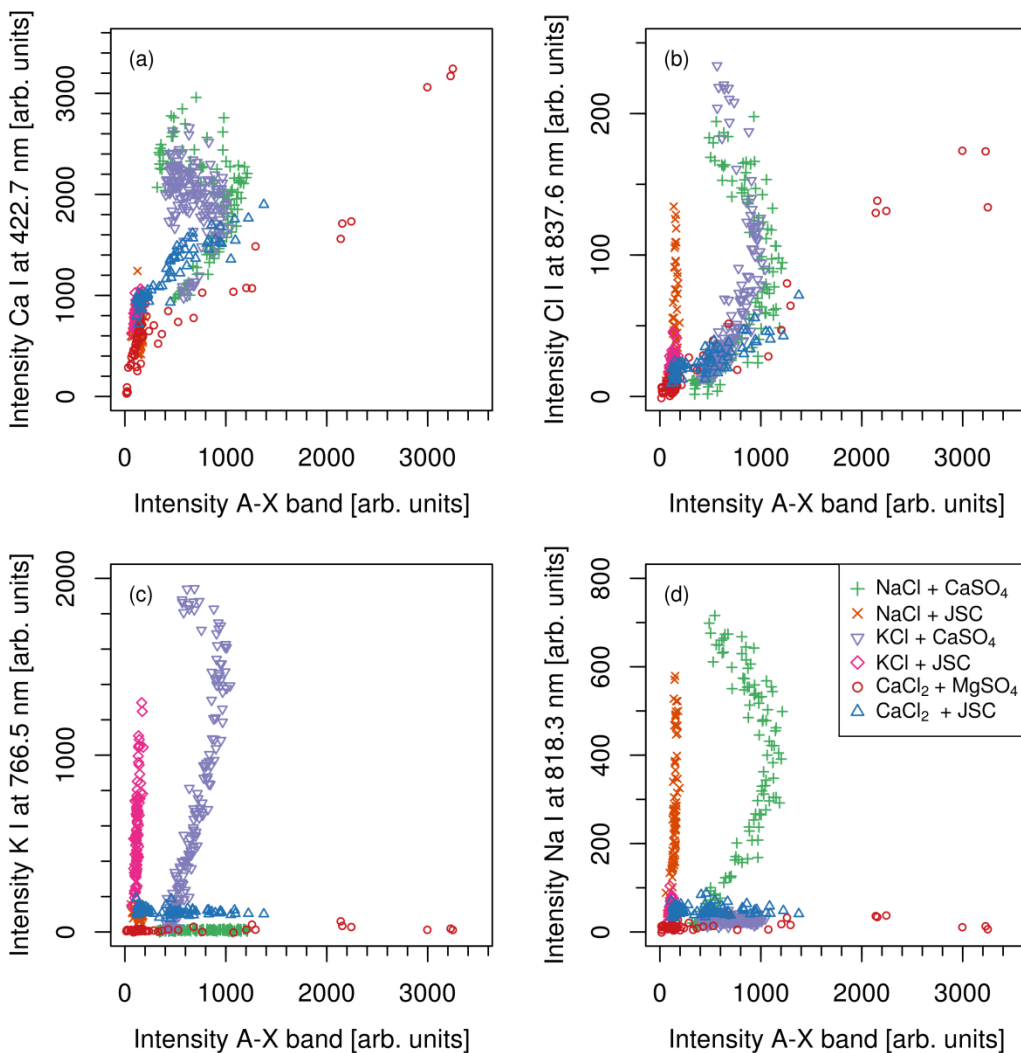


Figure 6: Intensity of the CaCl A-X band in dependence of the Ca and Cl concentrations for all mixed samples. Circles represent measurements with 350 ns delay time and 10  $\mu$ s integration time, triangles represent measurements with 0 ns delay time and 3 ms integration time. The same reaction kinetics model as in Fig. 4 is used to fit the CaCl

band intensities of all mixtures for both time gate settings. The same values are used for the majority of the fit parameters (see Section 4).

385



386

Figure 7: Intensities of Ca I, Cl I, K I, and Na I emission lines over the intensity of the CaCl A-X band for all mixed samples. It is possible to separate between samples and to estimate the composition based on the strength of the emission lines in relation to the strength of the CaCl band. (Legend in (d) applies to all plots.)

387

#### 388 4. Modeling of Reaction Kinetics

389 The CaCl molecules responsible for the molecular emissions in the spectra are formed inside  
390 the plasma by recombination of atoms and ions of Ca and Cl. The concentration of CaCl

391 molecules therefore depends on the concentrations of Ca and Cl in the plasma, which change  
 392 over time due to plasma expansion, cooling, and recombination of atoms and ions into molecules  
 393 like CaCl and CaO. In order to better understand these time-dependent processes inside the  
 394 plasma, a numerical model based on second-order reactions in a transient system was developed.  
 395 This was used to fit the measurement data. The second-order reaction rates are given by (e.g.  
 396 Laidler, 1977):

$$r_{CaCl}(t) = A_{CaCl} \exp(-E_{CaCl}/(k_B T(t))) [Ca](t) [Cl](t) \quad (2a)$$

$$r_{CaCl_2}(t) = A_{CaCl_2} \exp(-E_{CaCl_2}/(k_B T(t))) [CaCl](t) [Cl](t) \quad (2b)$$

398  
 399 Here,  $r_{CaCl}$  is the reaction rate of CaCl given the concentrations  $[Ca]$  and  $[Cl]$  and the  
 400 temperature  $T$ , with the pre-exponential factor  $A_{CaCl}$  and the activation energy  $E_{CaCl}$  for the  
 401 reaction. Equally,  $r_{CaCl_2}$  is the reaction rate of CaCl<sub>2</sub> given the concentrations  $[CaCl]$  and  $[Cl]$   
 402 and the temperature  $T$  with parameters  $A_{CaCl_2}$  and  $E_{CaCl_2}$ .  $k_B$  is the Boltzmann constant. Since  
 403 the density distribution in a LIBS plasma is different for each species (Aguilera et al., 2003; De  
 404 Giacomo et al., 2008; Lee et al., 1992), reactions between Ca and Cl can only take place in a  
 405 region where their density distributions overlap.  $T$  is the temperature of this overlap region. The  
 406 volume  $V$  of the overlap region is assumed to change linearly with time at a rate  $C_V$  starting with  
 407 an initial volume  $V_0$ :

$$V(t) = V_0 + C_V t \quad (3)$$

409  
 410 In order to model the decrease in concentration due to expansion of the plasma, concentration-  
 411 dependent expansion rates with expansion parameters  $B_{Ca}$ ,  $B_{Cl}$ , and  $B_{CaCl}$  were added for each  
 412 species. Then the changes in concentration of Ca, Cl, and CaCl can be modeled as follows:

$$d[Ca]/dt = -C_V/V(t)[Ca](t) - r_{CaCl}(t) - B_{Ca}[Ca](t) \quad (4a)$$

413

$$d[Cl]/dt = -C_V/V(t)[Cl](t) - r_{CaCl}(t) - r_{CaCl_2}(t) - B_{Cl}[Cl](t) \quad (4b)$$

$$d[CaCl]/dt = -C_V/V(t)[CaCl](t) + r_{CaCl}(t) - r_{CaCl_2}(t) - B_{CaCl}[CaCl](t) \quad (4c)$$

414

415 Initially, there is no CaCl present in the plasma plume, i.e.  $[CaCl](0) = 0$ . For Ca and Cl, it is  
 416 assumed that the initial stoichiometry of the plasma is equal to that of the sample under  
 417 investigation, i.e.  $[Ca](0) = n_{Ca}\rho_V$  and  $[Cl](0) = n_{Cl}\rho_V$ .  $n_{Ca}$  and  $n_{Cl}$  are the mole fractions of  
 418 Ca and Cl in the sample, while  $\rho_V$  is the number density of atoms and ions in the overlap region  
 419  $V_0$ . By iterating over small time steps of  $\Delta t = 1$  ns, the species concentrations at time  $t$  are  
 420 calculated. The CaCl band intensity  $I_{CaCl}$  is then proportional to the integral of the CaCl  
 421 concentration over the time gate:

422

$$I_{CaCl}(n_{Ca}, n_{Cl}) = C_S \int_{t_{del}}^{t_{del}+t_{gate}} [CaCl](t) dt \quad (5)$$

423

424 Here,  $t_{del}$  is the delay time and  $t_{gate}$  is the integration time of the measurement.  $C_S$  is a  
 425 parameter that relates the integral of the CaCl concentration to the band intensity.

426 The values for  $t_{del}$  and  $t_{gate}$  are determined by the measurement settings,  $n_{Ca}$  and  $n_{Cl}$  are  
 427 given by the stoichiometry of the samples. The temperature  $T(t)$  is calculated at each time using  
 428 Eq. (1) with the mean values of the parameters that have been found for Ca lines and Cl lines  
 429 (Table 4), since the overlap region is assumed to have a local temperature that is in between the  
 430 temperatures measured for each species. The remaining parameters in the equations above can be  
 431 divided into parameters which have the same value for all samples, and parameters which can  
 432 have different values for each sample. The reaction parameters  $A_{CaCl}$ ,  $E_{CaCl}$ ,  $A_{CaCl_2}$ , and  $E_{CaCl_2}$   
 433 only depend on the reacting species, so their values are assumed to be the same for all samples.  
 434 The expansion parameters  $B_{Ca}$ ,  $B_{Cl}$ , and  $B_{CaCl}$  mainly depend on the atmospheric pressure, and  
 435 should be the same for all samples as well.

436 The initial volume  $V_0$  of the reaction region, its rate of change  $C_V$ , the number density  $\rho_V$  of  
 437 atoms and ions in  $V_0$ , and  $C_S$  might be different for the samples, as variations in composition,  
 438 grain size, transparency, and hygroscopicity of the samples affect the amount of ablated material,

439 and likely the spatial distribution of elements inside the plasma plume as well. However, they are  
 440 assumed to reach similar values for samples that were mixed from the same two substances.  
 441 Therefore, the same value is used for all samples in this case.

442 All measurements from mixed samples and from pure  $\text{CaCl}_2$  were fitted with the model  
 443 described above. The best-fit parameter values obtained for the reaction parameters and the  
 444 expansion parameters are shown in Table 5. The fit describes the measurements very well, as it  
 445 accurately follows both the temporal evolution of the band intensity in pure  $\text{CaCl}_2$  (Fig. 4a) as  
 446 well as the changes in concentration for all mixed samples (Fig. 6). Differences of the intensity  
 447 curves for both measurement time settings are also accurately described by the model. The  
 448 adjusted coefficient of determination,  $R_{adj}^2$ , ranges from  $R_{adj}^2 = 0.86$  for the mixture of NaCl  
 449 and JSC to  $R_{adj}^2 = 0.99$  for the mixture of NaCl and  $\text{CaSO}_4$ , and reaches  $R_{adj}^2 = 0.96$  for the  
 450 complete fit of all samples. This demonstrates the strong correlation between observed and fitted  
 451 values for all mixtures.

452 The results from the fit with a reaction kinetics model indicate that the band intensity is linked  
 453 not only to the initial concentrations of Ca and Cl in the plasma, but also to the changes of these  
 454 values as the plasma expands and cools, and as the two species react with each other and with  
 455 other species in the plasma. The resulting behavior over time and for varying compositions is  
 456 complex. While calibration curves are assumed to be linear for atomic and ionic emissions  
 457 without self-absorption, this assumption cannot be made for molecular bands. Even in mixtures  
 458 of  $\text{CaCl}_2$  and  $\text{MgSO}_4$  or  $\text{CaCl}_2$  and JSC, where Ca and Cl are correlated, the fit curve is not  
 459 completely linear ( $R_{adj}^2 = 0.971$  for the correlation between a linear function and the fit curve  
 460 for mixtures of  $\text{CaCl}_2$  and JSC).

461

Table 5: Fit parameters of the reaction kinetics model

Parameter	Description	Value
$E_{CaCl}$	CaCl activation energy	$-(11 \pm 1)$ eV
$E_{CaCl_2}$	$\text{CaCl}_2$ activation energy	$-(11 \pm 1)$ eV
$A_{CaCl}$	Pre-exponential factor for CaCl reaction	$(2.8 \pm 0.1) \times 10^{-8} \text{ m}^3\text{s}^{-1}$
$A_{CaCl_2}$	Pre-exponential factor for $\text{CaCl}_2$ reaction	$(1.6 \pm 0.1) \times 10^{-6} \text{ m}^3\text{s}^{-1}$
$B_{Cl}$	Cl expansion constant	$(0.37 \pm 0.01) \text{ s}^{-1}$
$B_{Ca}$	Ca expansion constant	$(2.57 \pm 0.01) \text{ s}^{-1}$

462

463 **5. Discussion**

464 The analysis of the MgCl band in MgCl<sub>2</sub> and in mixtures of CaCl<sub>2</sub> and MgSO<sub>4</sub> indicates that  
465 the detection of MgCl emissions in LIBS spectra measured at Martian conditions is not possible  
466 with the current configuration. The molecular band that was suspected to be an MgCl band was  
467 also visible in chlorine-free dunite, suggesting that at least a large part of the signal is caused by  
468 unknown molecular emissions. As the signal could not be detected in samples that did not  
469 contain Mg, it is likely the molecular band of MgO, MgOH, or another polyatomic molecule that  
470 contains Mg. It is unclear if the lack of a clear MgCl signal in MgCl<sub>2</sub> is the result of an emission  
471 rate that is significantly lower than that of similar diatomic molecules, or if MgCl does not form  
472 in LIBS plasma under Martian conditions at all. Further investigation of the formation of MgCl  
473 in LIBS plasma will be necessary in order to understand why no MgCl bands could be observed.

474 The reactions involved in the formation and the decrease of CaCl over time have been  
475 modeled based on reaction kinetics. According to this model, the concentration of CaCl in the  
476 plasma plume of pure CaCl<sub>2</sub> in Martian conditions increases until about one microsecond after  
477 breakdown. At this point, the concentration reaches a maximum and then slowly decreases due to  
478 reactions and recombination processes in the cooling and expanding plasma. As the band  
479 intensity is proportional to the integral of this concentration over the measurement time, it is  
480 possible to set a delay time of 250 ns to 500 ns without losing a significant amount of intensity.  
481 This is fortunate, as the continuum emission decreases quickly over time and is not observed  
482 after about 250 ns anymore. Since it will be possible with SuperCam to set delay times for the  
483 detector that covers the wavelength of the CaCl bands, a delay time between 250 ns and 500 ns is  
484 recommended for measurements of these bands in order to exclude the continuum emission from  
485 the measurement without reducing the band intensity. This approach is generally preferable  
486 compared to post-processing the data with baseline removal algorithms, as it guarantees that no  
487 significant information is lost. Molecular bands, which cover a wide range of wavelengths,  
488 cannot always be separated from the baseline easily.

489 The measurements of the A–X band intensities in mixed samples confirm that the  
490 concentration of CaCl in the plasma strongly depends on the concentrations of both elements

491 (Fig. 6). Therefore, a one-dimensional, linear relationship between the chlorine concentration  
492 and the CaCl band intensity cannot be assumed. Even in mixtures where the Ca concentration  
493 increases proportionally to the Cl concentration, neither the observed nor the calculated band  
494 intensities depend linearly on the Cl due to the influence of the Ca concentration. In mixtures  
495 where they are anti-correlated, the band intensity instead quickly reaches a maximum and then  
496 slowly decreases. The curves are asymmetric, with the maximum at relatively small Cl  
497 concentrations and high Ca concentrations. The exact location of the maximum not only depends  
498 on the specific concentrations of Ca and Cl in the sample, but also on the delay time of the  
499 measurement.

500 Since it was possible to fit all samples with the same model, with the majority of the  
501 parameters values set equal for all samples, it seems that the overall composition of the  
502 investigated samples does not significantly impact the formation of CaCl, as long as Ca and Cl  
503 are present in sufficient concentrations. However, it was necessary to set volume parameters for  
504 each mixture separately. This suggests that the spatial distribution as well as movement and  
505 collisions of the species inside the plasma plume are affected by the sample composition.

506 In samples that contained both Mg and Ca as reaction partners for Cl, no decrease of the CaCl  
507 band intensity could be observed, which suggests that MgCl formation does not have a large  
508 impact on the Cl concentration in the plasma. It is possible that recombination of Ca with other  
509 elements in the plasma has a larger impact on the CaCl formation than recombination of Cl with  
510 other elements in the plasma. For an investigation of this effect, CaCl bands and CaF bands can  
511 be measured in spectra of mixed samples containing Ca, Cl, and F at varying concentrations.  
512 Since CaF emits very strongly even at low concentrations, formation of CaF might be preferred  
513 over the formation of CaCl. In this case, a strong dependence of the CaCl band intensity on F  
514 concentration is expected. Experiments with samples containing all three species at varying  
515 concentrations will be performed in a future study in order to test this hypothesis.

516 The activation energies for CaCl and for CaCl<sub>2</sub> listed in Table 5 are negative, suggesting that  
517 the reaction rate increases as the plasma cools, as is the case for exothermic reactions. However,  
518 they might indirectly describe influences that were not explicitly covered by the model.  
519 Examples include the spatial distribution of the elements inside the plasma over time or spatial  
520 temperature differences. Especially the observed difference of the temperature values measured  
521 using Ca lines and Cl lines indicates that these species are spatially separated from one another,

522 so that CaCl formation might only occur in an intermediate reaction region. In this case, special  
523 conditions may apply which have to be considered before calculating activation energies.  
524 Spatially resolved measurements of the LIBS plasma could help to better understand these  
525 influences and to adjust the model accordingly.

526 The results of this study explain why emission lines from both Ca and Cl might be visible in a  
527 spectrum even if no CaCl bands are observed. Since Ca II emission lines can be very strong even  
528 at low concentrations, a sample with a low amount of Ca and a high amount of Cl may show  
529 these emission lines, but the amount of Ca may not be sufficient to produce CaCl emission that  
530 can be detected. With regard to ChemCam, this may be the case for sediments of calcium-free  
531 chlorides in Martian soil with a low concentration of Ca, equivalent to the mixtures of NaCl and  
532 KCl with JSC Mars-1A. Likewise, high intensities of the CaCl bands do not necessarily indicate  
533 high concentrations of chlorine, as the band intensities will also be high if there is a high amount  
534 of Ca, but only a moderate amount of Cl. Estimations of the sample composition can be made by  
535 comparing the intensity of the CaCl band to that of the Ca emissions and those of other potential  
536 cations, which can usually be detected easily. As the concentrations of Ca and Cl are limited by  
537 the stoichiometry of the molecules in the composition, the strongest signals are only produced by  
538 a small number of possible compositions, which allow for high concentrations of both species.  
539 Meanwhile, spectra of calcium-free salts such as NaCl or KCl will also feature strong emissions  
540 of the cation.

541 The physical model for the calculation of the CaCl band intensity that has been presented in  
542 this study is at the moment not suited for the quantification of chlorine in Martian data, as it  
543 depends on unknown plasma parameters such as the volume of the overlap region of Ca and Cl  
544 in the plasma. In order to improve the model, the density distributions of Ca and Cl in a transient  
545 plasma plume need to be investigated for samples of different mixtures and for samples with  
546 varying homogeneity. This will be investigated in future studies with a spatially and temporally  
547 resolved LIBS setup. However, it is uncertain whether this physical model will allow for a more  
548 accurate quantification of Cl than an empirical approach based on multivariate data analysis.  
549 With multivariate data analysis of the complete spectrum, the interdependencies between  
550 multiple signals in the spectra can be taken into account, which should result in an accurate  
551 identification of the sample composition. In this context, the signals of both CaCl bands provide  
552 important information that makes the quantification of Cl possible even when no Cl signals can

553 be detected. At the moment, this kind of multivariate approach is probably the most reliable way  
554 to get accurate estimates of the Cl concentration and is highly recommended over a direct  
555 quantification of Cl using the CaCl band intensity.

## 556 **6. Conclusion**

557 Molecular emissions of MgCl and CaCl in LIBS spectra were investigated under Martian  
558 conditions in order to examine their potential for the quantification of Cl. It was shown that  
559 MgCl emissions are not suited for the quantification of chlorine under Martian conditions, as  
560 they could not be observed even in spectra of pure MgCl<sub>2</sub>. It is therefore unclear whether any  
561 MgCl has formed in the LIBS plasma at all. In contrast, the formation of CaCl was observed for  
562 all investigated samples containing sufficient amounts of Ca and Cl. The intensity of the CaCl  
563 bands is highly dependent on the concentrations of both Ca and Cl in the sample, however, and  
564 will decrease in intensity if either of the elements is too low in concentration. The dependence is  
565 asymmetric, favoring high concentrations of Ca over high concentrations of Cl due to a higher  
566 expansion rate of Ca. The highest concentration of CaCl in the plasma is reached after about 1 μs,  
567 which allows setting short delay times that filter out the continuum emission with only a minimal  
568 loss of CaCl band intensity. Using a reaction kinetics model, it was possible to fit multiple  
569 samples of varying composition with the same reaction and expansion parameters, resulting in a  
570 description of CaCl formation over time in dependence of the concentrations of Ca and Cl. Based  
571 on these results, a spatial separation of Ca and Cl inside the plasma seems likely and will be  
572 investigated in a future study. An investigation of the influence of other potential reaction  
573 partners of Ca on the intensity of CaCl bands would be very interesting as well, but went beyond  
574 the scope of this study. Especially fluorine is of high interest in the context of Martian  
575 exploration, as CaF emissions in LIBS spectra are very intense and have already been observed  
576 with ChemCam. The investigation of CaCl and CaF formation in samples containing varying  
577 amounts of Ca, Cl, and F will be addressed in a future study.

578 The results of this study provide insight that is important for the evaluation and interpretation  
579 of signals from molecular bands in LIBS spectra measured by ChemCam or SuperCam. Since  
580 halogens like Cl and F are difficult to detect with LIBS, they can often only be detected because  
581 of molecular bands of CaCl and CaF in spectra of Martian targets. However, as this study shows,  
582 a strong CaCl signal is not directly correlated with a high amount of Cl, and the absence of CaCl

583 bands does not necessarily indicate a lack of Cl. The study underlines the necessity of moving  
584 beyond the univariate approach for elements which can only be observed by molecular emission.  
585 Due to the strong interdependencies of the elemental emission lines and the molecular bands,  
586 multivariate analysis of the spectra is crucial for the quantification of these elements and for an  
587 accurate identification of the mineralogical composition of the corresponding target. Due to the  
588 importance of halogenic signals in the research of our solar system, it is important to understand  
589 the processes behind halogenic molecular emission in LIBS spectra as LIBS becomes an  
590 increasingly prevalent technique for in situ planetary exploration.

## 591 **References**

- 592 Aguilera, J.A., Aragón, C., Bengoechea, J., 2003. Spatial characterization of laser-induced plasmas by  
593 deconvolution of spatially resolved spectra. *Appl. Opt.* 42, 5938–5946. doi:10.1364/AO.42.005938
- 594 Allen, C.C., Jager, K.M., Morris, R.V., Lindstrom, D.J., Lindstrom, M.M., Lockwood, J.P., 1998. Martian soil  
595 simulant available for scientific, educational study. *Eos Trans. Am. Geophys. Union* 79, 405–409.  
596 doi:10.1029/98EO00309
- 597 Anderson, D.E., Ehlmann, B.L., Forni, O., Clegg, S.M., Cousin, A., Thomas, N.H., Lasue, J., Delapp, D.M.,  
598 McInroy, R.E., Gasnault, O., Dyar, M.D., Schröder, S., Maurice, S., Wiens, R.C., 2017. Characterization of  
599 LIBS emission lines for the identification of chlorides, carbonates, and sulfates in salt/basalt mixtures for  
600 the application to MSL ChemCam data. *J. Geophys. Res. Planets* 122, 2016JE005164.  
601 doi:10.1002/2016JE005164
- 602 Aragón, C., Aguilera, J.A., 2008. Characterization of laser induced plasmas by optical emission spectroscopy: A  
603 review of experiments and methods. *Spectrochim. Acta Part B At. Spectrosc.* 63, 893–916.  
604 doi:10.1016/j.sab.2008.05.010
- 605 Arp, Z.A., Cremers, D.A., Harris, R.D., Oschwald, D.M., Parker, G.R., Wayne, D.M., 2004. Feasibility of  
606 generating a useful laser-induced breakdown spectroscopy plasma on rocks at high pressure: preliminary  
607 study for a Venus mission. *Spectrochim. Acta Part B At. Spectrosc.* 59, 987–999.  
608 doi:10.1016/j.sab.2004.05.004
- 609 Bish, D.L., Blake, D.F., Vaniman, D.T., Chipera, S.J., Morris, R.V., Ming, D.W., Treiman, A.H., Sarrazin, P.,  
610 Morrison, S.M., Downs, R.T., Achilles, C.N., Yen, A.S., Bristow, T.F., Crisp, J.A., Morookian, J.M.,  
611 Farmer, J.D., Rampe, E.B., Stolper, E.M., Spanovich, N., Team, M.S., 2013. X-ray Diffraction Results  
612 from Mars Science Laboratory: Mineralogy of Rocknest at Gale Crater. *Science* 341, 1238932.  
613 doi:10.1126/science.1238932
- 614 Clegg, S.M., Mangold, N., Le Mouélic, S., Olilla, A., Anderson, R., Blaney, D.L., Clark, B., Cousin, A., Dyar, M.D.,  
615 Ehlmann, B.L., Fabre, C., Forni, O., Lasue, J., Meslin, P.-Y., Schroder, S., Sirven, J.B., Vaniman, D.T.,  
616 Maurice, S., Wiens, R.C., MSL Science Team, 2013. High Calcium Phase Observations at Rocknest with  
617 ChemCam. Presented at the 44th Lunar and Planetary Science Conference.
- 618 Cousin, A., Schröder, S., Nachon, M., Gasnault, O., Maurice, S., Wiens, R.C., 2015. Quantification of chlorine on  
619 Mars using the ChemCam instrument. Presented at the EMSLIBS 2015.
- 620 Cremers, D.A., Radziemski, L.J., 2006. Basics of the LIBS Plasma, in: *Handbook of Laser-Induced Breakdown*  
621 *Spectroscopy*. John Wiley & Sons, Ltd, pp. 23–52. doi:10.1002/0470093013.ch2
- 622 Cremers, D.A., Radziemski, L.J., 1983. Detection of Chlorine and Fluorine in Air by Laser-Induced Breakdown  
623 Spectrometry. *Anal Chem U. S.* 55:8. doi:10.1021/ac00259a017
- 624 Cristoforetti, G., De Giacomo, A., Dell’Aglia, M., Legnaioli, S., Tognoni, E., Palleschi, V., Omenetto, N., 2010.  
625 Local Thermodynamic Equilibrium in Laser-Induced Breakdown Spectroscopy: Beyond the McWhirter  
626 criterion. *Spectrochim. Acta Part B At. Spectrosc.* 65, 86–95. doi:10.1016/j.sab.2009.11.005
- 627 D’Ammando, G., Pietanza, L.D., Colonna, G., Longo, S., Capitelli, M., 2010. Modelling spectral properties of non-  
628 equilibrium atomic hydrogen plasma. *Spectrochim. Acta Part B At. Spectrosc.* 65, 120–129.

629 De Giacomo, A., Dell'Aglio, M., Gaudiuso, R., Cristoforetti, G., Legnaioli, S., Palleschi, V., Tognoni, E., 2008.  
630 Spatial distribution of hydrogen and other emitters in aluminum laser-induced plasma in air and  
631 consequences on spatially integrated Laser-Induced Breakdown Spectroscopy measurements. *Spectrochim.*  
632 *Acta Part B At. Spectrosc.* 63, 980–987. doi:10.1016/j.sab.2008.06.010

633 De Giacomo, A., Gaudiuso, R., Dell'Aglio, M., Santagata, A., 2010. The role of continuum radiation in laser  
634 induced plasma spectroscopy. *Spectrochim. Acta Part B At. Spectrosc.* 65, 385–394.  
635 doi:10.1016/j.sab.2010.03.016

636 Dreibus, G., Wänke, H., 1987. Volatiles on Earth and Mars: A comparison. *Icarus* 71, 225–240. doi:10.1016/0019-  
637 1035(87)90148-5

638 Dreibus, G., Wänke, H., 1985. Mars, a volatile-rich planet. *Meteoritics* 20, 367–381.

639 Ehlmann, B.L., Edwards, C.S., 2014. Mineralogy of the Martian surface. *Annu. Rev. Earth Planet. Sci.* 42, 291–315.

640 Ehlmann, B.L., Mustard, J.F., Murchie, S.L., Bibring, J.-P., Meunier, A., Fraeman, A.A., Langevin, Y., 2011.  
641 Subsurface water and clay mineral formation during the early history of Mars. *Nature* 479, 53–60.  
642 doi:10.1038/nature10582

643 Filiberto, J., Treiman, A.H., 2009. Martian magmas contained abundant chlorine, but little water. *Geology* 37, 1087–  
644 1090. doi:10.1130/G30488A.1

645 Forni, O., Gaft, M., Toplis, M.J., Clegg, S.M., Maurice, S., Wiens, R.C., Mangold, N., Gasnault, O., Sautter, V., Le  
646 Mouélic, S., Meslin, P.-Y., Nachon, M., McInroy, R.E., Ollila, A.M., Cousin, A., Bridges, J.C., Lanza, N.L.,  
647 Dyar, M.D., 2015. First detection of fluorine on Mars: Implications for Gale Crater's geochemistry.  
648 *Geophys. Res. Lett.* 42, 2014GL062742. doi:10.1002/2014GL062742

649 Gaft, M., Nagli, L., Eliezer, N., Groisman, Y., Forni, O., 2014. Elemental analysis of halogens using molecular  
650 emission by laser-induced breakdown spectroscopy in air. *Spectrochim. Acta Part B At. Spectrosc.* 98, 39–  
651 47. doi:10.1016/j.sab.2014.05.011

652 Grotzinger, J.P., Crisp, J., Vasavada, A.R., Anderson, R.C., Baker, C.J., Barry, R., Blake, D.F., Conrad, P., Edgett,  
653 K., Ferdowski, B., Gellert, R., Gilbert, J.B., Golombek, M., Gómez-Elvira, J., Hassler, D.M., Jandura, L.,  
654 Litvak, M., Mahaffy, P., Maki, J., Meyer, M., Malin, M.C., Mitrofanov, I., Simmonds, J.J., Vaniman, D.,  
655 Welch, R.V., Wiens, R.C., 2012. Mars Science Laboratory Mission and Science Investigation. *Space Sci.*  
656 *Rev.* 170, 5–56. doi:10.1007/s11214-012-9892-2

657 Haberle, R.M., McKay, C.P., Schaeffer, J., Cabrol, N.A., Grin, E.A., Zent, A.P., Quinn, R., 2001. On the possibility  
658 of liquid water on present-day Mars. *J. Geophys. Res. Planets* 106, 23317–23326.  
659 doi:10.1029/2000JE001360

660 Hecht, M.H., Kounaves, S.P., Quinn, R.C., West, S.J., Young, S.M.M., Ming, D.W., Catling, D.C., Clark, B.C.,  
661 Boynton, W.V., Hoffman, J., DeFlores, L.P., Gospodinova, K., Kapit, J., Smith, P.H., 2009. Detection of  
662 Perchlorate and the Soluble Chemistry of Martian Soil at the Phoenix Lander Site. *Science* 325, 64–67.  
663 doi:10.1126/science.1172466

664 Keller, J.M., Boynton, W.V., Karunatillake, S., Baker, V.R., Dohm, J.M., Evans, L.G., Finch, M.J., Hahn, B.C.,  
665 Hamara, D.K., Janes, D.M., Kerry, K.E., Newsom, H.E., Reedy, R.C., Sprague, A.L., Squyres, S.W., Starr,  
666 R.D., Taylor, G.J., Williams, R.M.S., 2006. Equatorial and midlatitude distribution of chlorine measured by  
667 Mars Odyssey GRS. *J. Geophys. Res. Planets* 111, E03S08. doi:10.1029/2006JE002679

668 Knight, A.K., Scherbarth, N.L., Cremers, D.A., Ferris, M.J., 2000. Characterization of Laser-Induced Breakdown  
669 Spectroscopy (LIBS) for Application to Space Exploration. *Appl. Spectrosc.* 54, 331–340.  
670 doi:10.1366/0003702001949591

671 Laidler, K.J., 1977. Chemical kinetics, in: *Chemical Kinetics*. McGraw-Hill.

672 Lee, Y.-I., Sawan, S.P., Thiem, T.L., Teng, Y.-Y., Sneddon, J., 1992. Interaction of a Laser Beam with Metals. Part  
673 II: Space-Resolved Studies of Laser-Ablated Plasma Emission. *Appl. Spectrosc.* 46, 436–441.

674 Massé, M., Bourgeois, O., Le Mouélic, S., Verpoorter, C., Le Deit, L., Bibring, J.P., 2010. Martian polar and  
675 circum-polar sulfate-bearing deposits: Sublimation tills derived from the North Polar Cap. *Icarus* 209, 434–  
676 451. doi:10.1016/j.icarus.2010.04.017

677 Maurice, S., Clegg, S.M., Wiens, R.C., Gasnault, O., Rapin, W., Forni, O., Cousin, A., Sautter, V., Mangold, N.,  
678 Deit, L.L., Nachon, M., Anderson, R.B., Lanza, N.L., Fabre, C., Payré, V., Lasue, J., Meslin, P.-Y.,  
679 Lèveillé, R.J., Barraclough, B.L., Beck, P., Bender, S.C., Berger, G., Bridges, J.C., Bridges, N.T., Dromart,  
680 G., Dyar, M.D., Francis, R., Frydenvang, J., Gondet, B., Ehlmann, B.L., Herkenhoff, K.E., Johnson, J.R.,  
681 Langevin, Y., Madsen, M.B., Melikechi, N., Lacour, J.-L., Mouélic, S.L., Lewin, E., Newsom, H.E., Ollila,  
682 A.M., Pinet, P., Schröder, S., Sirven, J.-B., Tokar, R.L., Toplis, M.J., d'Uston, C., Vaniman, D.T.,  
683 Vasavada, A.R., 2016. ChemCam activities and discoveries during the nominal mission of the Mars  
684 Science Laboratory in Gale crater, Mars. *J. Anal. At. Spectrom.* 31, 863–889. doi:10.1039/C5JA00417A

685 Maurice, S., Wiens, R.C., Anderson, R., Beyssac, O., Bonal, L., Clegg, S., DeFlores, L., Dromart, G., Fischer, W.,  
686 Forni, O., Gasnault, O., Grotzinger, J., Johnson, J., Martinez-Frias, J., Mangold, N., McLennan, S.,  
687 Montmessin, F., Rull, F., Sharma, S., Fouchet, T., Poulet, F., SuperCam Team, 2015. Science Objectives of  
688 the SuperCam Instrument for the Mars2020 Rover. Presented at the 46th Lunar and Planetary Science  
689 Conference.

690 Maurice, S., Wiens, R.C., Saccoccio, M., Barraclough, B., Gasnault, O., Forni, O., Mangold, N., Baratoux, D.,  
691 Bender, S., Berger, G., Bernardin, J., Berthé, M., Bridges, N., Blaney, D., Bouyé, M., Caïs, P., Clark, B.,  
692 Clegg, S., Cousin, A., Cremers, D., Cros, A., DeFlores, L., Derycke, C., Dingler, B., Dromart, G., Dubois,  
693 B., Dupieux, M., Durand, E., d'Uston, L., Fabre, C., Faure, B., Gaboriaud, A., Gharsa, T., Herkenhoff, K.,  
694 Kan, E., Kirkland, L., Kouach, D., Lacour, J.-L., Langevin, Y., Lasue, J., Mouélic, S.L., Lescure, M.,  
695 Lewin, E., Limonadi, D., Manhès, G., Mauchien, P., McKay, C., Meslin, P.-Y., Michel, Y., Miller, E.,  
696 Newsom, H.E., Orttner, G., Paillet, A., Parès, L., Parot, Y., Pérez, R., Pinet, P., Poitrasson, F., Quertier, B.,  
697 Sallé, B., Sotin, C., Sautter, V., Séran, H., Simmonds, J.J., Sirven, J.-B., Stiglich, R., Striebig, N., Thocaven,  
698 J.-J., Toplis, M.J., Vaniman, D., 2012. The ChemCam Instrument Suite on the Mars Science Laboratory  
699 (MSL) Rover: Science Objectives and Mast Unit Description. *Space Sci. Rev.* 170, 95–166.  
700 doi:10.1007/s11214-012-9912-2

701 Meslin, P.-Y., Gasnault, O., Forni, O., Schröder, S., Cousin, A., Berger, G., Clegg, S.M., Lasue, J., Maurice, S.,  
702 Sautter, V., Mouélic, S.L., Wiens, R.C., Fabre, C., Goetz, W., Bish, D., Mangold, N., Ehlmann, B., Lanza,  
703 N., Harri, A.-M., Anderson, R., Rampe, E., McConnochie, T.H., Pinet, P., Blaney, D., Léveillé, R., Archer,  
704 D., Barraclough, B., Bender, S., Blake, D., Blank, J.G., Bridges, N., Clark, B.C., DeFlores, L., Delapp, D.,  
705 Dromart, G., Dyar, M.D., Fisk, M., Gondet, B., Grotzinger, J., Herkenhoff, K., Johnson, J., Lacour, J.-L.,  
706 Langevin, Y., Leshin, L., Lewin, E., Madsen, M.B., Melikechi, N., Mezzacappa, A., Mischna, M.A.,  
707 Moores, J.E., Newsom, H., Ollila, A., Perez, R., Renno, N., Sirven, J.-B., Tokar, R., Torre, M. de la,  
708 d'Uston, L., Vaniman, D., Yingst, A., Team, M.S., 2013. Soil Diversity and Hydration as Observed by  
709 ChemCam at Gale Crater, Mars. *Science* 341, 1238670. doi:10.1126/science.1238670

710 Möhlmann, D., Thomsen, K., 2011. Properties of cryobrine on Mars. *Icarus* 212, 123–130.  
711 doi:10.1016/j.icarus.2010.11.025

712 Osterloo, M.M., Hamilton, V.E., Bandfield, J.L., Glotch, T.D., Baldrige, A.M., Christensen, P.R., Tornabene, L.L.,  
713 Anderson, F.S., 2008. Chloride-Bearing Materials in the Southern Highlands of Mars. *Science* 319, 1651–  
714 1654. doi:10.1126/science.1150690

715 Pearse, R.W.B., Gaydon, A.G., 1976. *Identification of Molecular Spectra*. Chapman and Hall.

716 Peret, L., Gasnault, O., Dingler, R., Langevin, Y., Bender, S., Blaney, D., Clegg, S., Clewans, C., Delapp, D., Donny,  
717 C.M., Johnstone, S., Little, C., Lorigny, E., McInroy, R., Maurice, S., Mittal, N., Pavri, B., Perez, R.,  
718 Wiens, R.C., Yana, C., 2016. Restoration of the Autofocus capability of the ChemCam instrument onboard  
719 the Curiosity rover, in: *SpaceOps 2016 Conference*. American Institute of Aeronautics and Astronautics.  
720 doi:10.2514/6.2016-2539

721 Querbach, J., 1930. Über die Spektren von Fe, La, Ca, Ba, Sr, Mg und ihrer Verbindungen im nahen Ultrarot. *Z. Für*  
722 *Phys. Hadrons Nucl.* 60, 109–124.

723 Rennó, N.O., Bos, B.J., Catling, D., Clark, B.C., Drube, L., Fisher, D., Goetz, W., Hviid, S.F., Keller, H.U., Kok,  
724 J.F., Kounaves, S.P., Leer, K., Lemmon, M., Madsen, M.B., Markiewicz, W.J., Marshall, J., McKay, C.,  
725 Mehta, M., Smith, M., Zorzano, M.P., Smith, P.H., Stoker, C., Young, S.M.M., 2009. Possible physical and  
726 thermodynamical evidence for liquid water at the Phoenix landing site. *J. Geophys. Res. Planets* 114,  
727 E00E03. doi:10.1029/2009JE003362

728 Schröder, S., Pavlov, S.G., Rauschenbach, I., Jessberger, E.K., Hübers, H.-W., 2013. Detection and identification of  
729 salts and frozen salt solutions combining laser-induced breakdown spectroscopy and multivariate analysis  
730 methods: A study for future martian exploration. *Icarus* 223, 61–73. doi:10.1016/j.icarus.2012.11.011

731 Smith, P.H., Tamppari, L.K., Arvidson, R.E., Bass, D., Blaney, D., Boynton, W.V., Carswell, A., Catling, D.C.,  
732 Clark, B.C., Duck, T., DeJong, E., Fisher, D., Goetz, W., Gunnlaugsson, H.P., Hecht, M.H., Hipkin, V.,  
733 Hoffman, J., Hviid, S.F., Keller, H.U., Kounaves, S.P., Lange, C.F., Lemmon, M.T., Madsen, M.B.,  
734 Markiewicz, W.J., Marshall, J., McKay, C.P., Mellon, M.T., Ming, D.W., Morris, R.V., Pike, W.T., Renno,  
735 N., Staufer, U., Stoker, C., Taylor, P., Whiteway, J.A., Zent, A.P., 2009. H<sub>2</sub>O at the Phoenix Landing Site.  
736 *Science* 325, 58–61. doi:10.1126/science.1172339

737 Taylor, G.J., Martel, L.M.V., Karunatillake, S., Gasnault, O., Boynton, W.V., 2010. Mapping Mars geochemically.  
738 *Geology* 38, 183–186. doi:10.1130/G30470.1

739 Wiens, R.C., Maurice, S., Barraclough, B., Saccoccio, M., Barkley, W.C., Bell, J.F., Bender, S., Bernardin, J.,  
740 Blaney, D., Blank, J., Bouyé, M., Bridges, N., Bultman, N., Caïs, P., Clanton, R.C., Clark, B., Clegg, S.,

741 Cousin, A., Cremers, D., Cros, A., DeFlores, L., Delapp, D., Dingler, R., D'Uston, C., Dyar, M.D., Elliott,  
742 T., Enemark, D., Fabre, C., Flores, M., Forni, O., Gasnault, O., Hale, T., Hays, C., Herkenhoff, K., Kan, E.,  
743 Kirkland, L., Kouach, D., Landis, D., Langevin, Y., Lanza, N., LaRocca, F., Lasue, J., Latino, J., Limonadi,  
744 D., Lindensmith, C., Little, C., Mangold, N., Manhes, G., Mauchien, P., McKay, C., Miller, E., Mooney, J.,  
745 Morris, R.V., Morrison, L., Nelson, T., Newsom, H., Ollila, A., Ott, M., Pares, L., Perez, R., Poitrasson, F.,  
746 Provost, C., Reiter, J.W., Roberts, T., Romero, F., Sautter, V., Salazar, S., Simmonds, J.J., Stiglich, R.,  
747 Storms, S., Striebig, N., Thocaven, J.-J., Trujillo, T., Ulibarri, M., Vaniman, D., Warner, N., Waterbury, R.,  
748 Whitaker, R., Witt, J., Wong-Swanson, B., 2012. The ChemCam Instrument Suite on the Mars Science  
749 Laboratory (MSL) Rover: Body Unit and Combined System Tests. *Space Sci. Rev.* 170, 167–227.  
750 doi:10.1007/s11214-012-9902-4  
751 Wiens, R.C., Maurice, S., Rull, F., SuperCam Team, 2016. SuperCam Remote Sensing on the Mars 2020 Rover:  
752 Science Goals and Overview. *LPI Contrib.* 1980, 4136.  
753